SEMARAK ILMU PUBLISHING

Semarak Engineering Journal

Journal homepage:
https://semarakilmu.my/index.php/sej/index
ISSN: 3036-0145



Finite Element-Based Structural Optimization and Safety Evaluation of an Eddy-Current Chassis Dynamometer for Motorcycles up to 200 cc

Mohd Mustaqim Tukiman[1], Aida Husna Ahmad[1], Mohd Firdaus Abas[1], Kazeem Babalola Olawale[2], Eliza M. Yusup[1], Shahrul Azmir Osman[1,*]

[1] Faculty of Mechanical and Manufacturing Engineering, Universiti Tun Hussein Onn Malaysia, 86400 Parit Raja, batu Pahat, Johor, Malaysia
[2] Department of Automobile Technology, Federal College of education (Technical) Bichi, Kano State, Nigeria

ARTICLE INFO

Article history:
Received 23 August 2026
Received in revised form 2 October 2026
Accepted 1 November 2026
Available online 18 November2026

Keywords:
Eddy-current chassis dynamometer; motorcycles up to 200 cc; finite element analysis; structural improvement; factor of safety (FoS); design evaluation

ABSTRACT

Motorcycle chassis dynamometers are tools for evaluating engine performance under workshop conditions. For motorcycles up to 200 cc, compact dynamometer structures must provide structural integrity while remaining material-efficient, manufacturable, and safe for workshop operation. This study presents a preliminary structural and safety-oriented evaluation of an eddy-current chassis dynamometer for motorcycles up to 200 cc. Three configurations with structural thicknesses of 6.0, 5.5, and 5.0 mm were modelled in SolidWorks and analysed using static finite element analysis under a uniformly distributed vertical load of 1400 N. Plain carbon steel, with a yield strength of 220.6 MPa, was selected based on availability, weldability, and suitability for fabrication. Structural performance was evaluated using von Mises stress, resultant displacement, equivalent strain, and factor of safety (FoS), while material efficiency and operational safety readiness were incorporated into a weighted multi-criteria design-selection framework. All configurations produced maximum stresses below the yield strength and minimum FoS values ranging from 2.3 to 4.2, exceeding the preliminary screening criterion of 2.0. Design 1 exhibited the lowest maximum von Mises stress of 52.80 MPa and highest FoS of 4.2. Design 2 showed a balanced response, with a maximum stress of 56.17 MPa, displacement of 0.862 mm, FoS of 3.9, and an 8.33% thickness reduction relative to the baseline. Design 3 achieved the greatest thickness reduction of 16.67% but recorded the highest stress of 96.33 MPa, displacement of 1.172 mm, and lowest FoS of 2.3. Nevertheless, Design 3 achieved the highest weighted score of 4.20 and was identified as the preferred preliminary configuration. The findings represent comparative static design screening rather than operational validation; dynamic and fatigue analyses, prototype fabrication, and experimental testing under representative operating conditions are required before practical implementation.

* *Corresponding author.*
E-mail address: shahrula@uthm.edu.my

https://doi.org/10.37934/sej.17.1.3661

1. Introduction

Motorcycles, particularly those with engine displacements below 200cc, are widely used for daily transportation in many developing countries because of their affordability, compactness, low operating cost, and flexibility in congested urban environments. The increasing use of motorcycles has also intensified the need for reliable engine performance assessment, especially in relation to power output, torque characteristics, fuel efficiency, and exhaust emissions. Accurate testing facilities are therefore required to support engine tuning, performance verification, emission assessment, and technical development for small-displacement motorcycles [1,2].

Chassis dynamometers are commonly used to evaluate vehicle and motorcycle performance under controlled operating conditions without removing the engine from the vehicle. In motorcycle applications, a chassis dynamometer allows the drive wheel to transfer torque to a roller system, enabling the measurement or estimation of engine speed, torque, power output, and related performance parameters. Among the available dynamometer technologies, eddy-current dynamometers are particularly suitable for small-displacement motorcycle testing because of their compact configuration, smooth load control, rapid braking response, and relatively low maintenance requirements [3,4]. In an eddy-current braking system, braking torque is generated by electromagnetic induction, in which the absorbed mechanical energy is converted into heat within the conductive rotating component. Consequently, the dynamometer structure and supporting components must be designed to withstand mechanical loading while ensuring safe, stable operation during testing. Excessive heat generation may also influence braking consistency, material behavior, torque prediction, and component reliability if it is not properly considered in the overall design [5-7].

Although chassis dynamometers are widely used in automotive testing, many commercial systems are primarily designed for larger vehicles and may not be suitable for motorcycles below 200cc. The differences in motorcycle size, mass, tire contact behavior, power output, handling characteristics, and workshop space limitations require a more compact and application-specific dynamometer structure. For small-scale workshops and laboratory environments, the dynamometer must not only provide adequate testing capability but also ensure sufficient structural strength, material efficiency, ease of fabrication, and operational safety. During motorcycle testing, the structure is subjected to vertical loading from the motorcycle, reaction forces from the rotating roller and braking system, vibration, heat exposure, and potential safety hazards associated with rotating components, tire-roller interaction, vehicle restraint, and fire risk. Therefore, a systematic, structural, and safety-oriented design approach is necessary to ensure the dynamometer operates safely while remaining compact and cost-effective.

Previous studies on motorcycle and small-vehicle dynamometer systems have generally emphasized measurement capability, engine performance, torque, speed, power, and emissions. However, less attention has been given to the integrated evaluation of structural adequacy, material usage, and practical safety provisions during the early design stage. Inadequate structural stiffness may cause excessive deformation, misalignment, unstable tire-roller contact, and reduced repeatability of performance measurement. Similarly, insufficient safety consideration may increase operational risk during testing, especially when the motorcycle is operated under stationary but loaded conditions. These risks include exposure to rotating rollers, high mechanical loads, engine heat, braking system heat, and possible fire-related incidents. Hence, practical safety features, clear operator monitoring arrangements, and emergency preparedness should be considered together with structural performance during the design process [1,8-10].

FEA provides an effective method for evaluating the structural performance of a dynamometer before fabrication. Through FEA, critical stress regions, deformation behavior, strain response, and FoS safety can be assessed under defined loading and boundary conditions. This approach is particularly useful for comparing alternative designs and identifying whether material thickness can be reduced without compromising structural safety. For a compact motorcycle chassis dynamometer, FEA-based design evaluation can support material efficiency while ensuring that the frame remains within the elastic range under the intended loading condition.

To address these requirements, this study presents a structural and safety-oriented optimization of an eddy-current chassis dynamometer designed for motorcycles with engine capacities up to 200cc. 3 design alternatives were developed using SolidWorks and evaluated through static FEA under an applied vertical load of 1400N. The designs were compared based on von Mises stress, displacement, strain response, and FoS. In addition, a weighted multi-criteria decision-making method was used to select the most suitable configuration, considering structural safety, material efficiency, and practical operational safety provisions. This approach enables the final design to be selected not only on structural robustness but also on a balance between mechanical adequacy, reduced material use, and safe workshop operation.

This study aims to evaluate and select a structurally adequate, material-efficient eddy-current chassis dynamometer configuration for motorcycles with engine capacities up to 200cc. The engineering contribution of this work lies not in the application of FEA itself, which is a well-established structural assessment method, but in its systematic integration into an application-specific design-selection framework for a compact motorcycle dynamometer. 3 progressively reduced structural thicknesses of 6.0mm, 5.5mm, and 5.0 mm are assessed under identical loading, boundary, material, and mesh-verification conditions to quantify the trade-off between material reduction and the resulting structural safety margin. The structural responses are subsequently integrated with material-efficiency and operational-safety criteria through a weighted multi-criteria evaluation. This framework enables a clear distinction between the configuration that provides the highest structural conservatism and the configuration that offers the most appropriate overall engineering balance. Consequently, the study establishes a systematic basis for selecting a compact chassis dynamometer configuration in which structural adequacy, material utilization, and practical workshop safety are evaluated concurrently rather than as independent design considerations.

2. Literature Review

2.1 Motorcycle Chassis Dynamometer Systems

A chassis dynamometer is an important testing system used to evaluate vehicle or motorcycle performance under controlled operating conditions. Unlike an engine dynamometer, which requires the engine to be tested as a separate power unit, a chassis dynamometer allows the motorcycle to remain assembled. In this arrangement, the motorcycle drive wheel transmits torque to a roller or drum system, enabling the evaluation of vehicle-level performance. The measured output therefore represents the combined effect of the engine, transmission, final drive, wheel, tire roller contact, and drivetrain losses. This makes the chassis dynamometer highly practical for workshop and laboratory applications, particularly for assessing engine speed, torque, power, fuel consumption, exhaust emissions, and tuning performance without removing the engine from the motorcycle [11-14].

For motorcycles up to 200cc, chassis dynamometer design requires particular attention because these vehicles differ from larger vehicles in size, mass, power output, handling behavior, wheelbase, and tire-loading characteristics. A compact motorcycle dynamometer must be able to support the motorcycle safely while maintaining stable tire-roller contact during testing. At the same time, it must

remain cost-effective, simple to fabricate, and suitable for space-limited workshop environments. Therefore, the design of a small-displacement motorcycle chassis dynamometer should focus not only on measurement capability but also on structural rigidity, material efficiency, safety, and practical operation.

2.2 Eddy-Current Dynamometer and Braking Characteristics

Several types of dynamometer systems have been used for vehicle and motorcycle testing, including inertia, hydraulic or water-brake, alternating-current electric, and eddy-current dynamometers. For small-displacement motorcycle testing, eddy-current dynamometers offer several advantages, including compact construction, smooth braking control, fast load response, and relatively low maintenance. The braking effect in an eddy-current dynamometer is produced through electromagnetic induction. When a conductive disc or rotor moves through a magnetic field, eddy currents are generated, and the interaction between the magnetic field and induced currents produces braking torque. This allows controllable loading to be applied to the motorcycle during performance testing.

Previous studies have demonstrated the practical use of chassis dynamometers in 2-wheeler and small-vehicle applications. Maniar et al., [15] investigated a portable 2-wheeler dynamometer test rig, while Arifwardana et al., [16] applied a chassis dynamometer for hybrid 2-wheeler characterization [15,16]. Dai also used dynamometer-based testing for performance verification of a motorcycle clutch transmission system [17]. These studies show that chassis dynamometers are useful for evaluating 2-wheeler performance, drivetrain characteristics, and power transmission behavior. However, many of these studies focused primarily on testing capabilities and performance metrics, with less emphasis on structural optimization, safety readiness, and material-efficient design for compact, workshop-scale systems.

A key limitation of eddy-current braking systems is the generation of heat. The mechanical energy absorbed by the braking system is converted into heat within the conductive disc, stator, coil, and surrounding components. If this heat is not properly managed, the rise in temperature may affect electrical conductivity, magnetic behavior, coil resistance, and braking torque stability. As a result, braking performance, torque prediction, and measurement repeatability may be affected. Continuous heat exposure may also accelerate material degradation and reduce the reliability of nearby sensors or electronic components [18-20]. Although thermal performance is not the primary structural output of the present study, it remains an important operational consideration in the design of eddy-current dynamometer systems.

2.3 Thermal and Operational Considerations in Motorcycle Testing

Thermal management is an important consideration in dynamometer operation because the motorcycle is tested in a stationary condition. Under actual road operation, the motorcycle engine and related components receive natural airflow as the vehicle moves. However, during chassis dynamometer testing, this natural airflow is limited or absent, especially when the motorcycle remains fixed on the roller system. As a result, engine, lubricant, coolant, and braking system temperatures may increase during extended testing, which can affect performance consistency, operator safety, and the durability of mechanical and electronic components. Putra et al., showed that heat generation in a unipolar axial eddy-current brake increased the disc surface temperature and reduced braking torque performance, with experimental torque decreasing from 6.63Nm at 25℃ to 6.23Nm at 45℃ [18].

This finding confirms that increasing temperature can influence eddy-current braking behavior. This finding confirms that increasing temperature can influence eddy-current braking behavior. Further studies by S. Zhang et al., [7] and Fu et al., [21] also highlighted the importance of controlling temperature rise in eddy-current braking systems through suitable cooling strategies and electromagnetic–thermal design considerations [7,21]. In motorcycle chassis dynamometer applications, auxiliary forced-air cooling is commonly required to maintain stable engine operation during stationary testing. Cooling fans may therefore be included as supporting equipment to reduce overheating risk and improve operational stability during repeated or extended test sessions [22,23].

2.4 Structural Design Requirements and Finite Element Analysis

Structural performance is a fundamental requirement in the design of a motorcycle chassis dynamometer. The dynamometer frame must support the motorcycle, roller assembly, braking unit, mounting components, and auxiliary equipment while maintaining sufficient stiffness under loading. Excessive deformation may affect roller alignment, tire-roller contact, load transfer, and overall measurement repeatability. For this reason, the structural design must provide adequate strength and rigidity while avoiding unnecessary material usage. This is particularly important for compact dynamometers intended for small workshops, where cost, weight, fabrication simplicity, and space efficiency are important design considerations.

Material selection for a dynamometer frame requires consideration of several competing criteria, including mechanical strength, stiffness, structural mass, corrosion resistance, manufacturability, material availability, and cost. Although materials with higher specific strength may offer opportunities for reducing structural mass, their practical suitability also depends on fabrication complexity, joining requirements, cost, and the intended operating environment. For the present workshop-scale dynamometer, material selection was therefore approached primarily from the perspectives of manufacturability and structural adequacy, while material efficiency was investigated through controlled variation of the structural thickness.

The roller support and frame structure must be designed to resist static and operational loads during motorcycle testing. Poor structural stiffness can lead to local deflection, vibration sensitivity, and misalignment between the tire and roller. These conditions may influence torque transfer and reduce the repeatability of test results. Bagaskoro and Aryadi (2024), and Doan et al., (2022) emphasized the importance of roller support, tire-roller contact, and structural integrity in chassis dynamometer systems [13,24]. Therefore, structural analysis is necessary during the design stage to identify critical stress regions and ensure that the dynamometer can safely withstand the intended loading condition.

FEA is widely used in engineering design because it enables the evaluation of stress, displacement, strain, and FoS before fabrication. It is especially useful for comparing several design alternatives and identifying whether material thickness can be reduced while maintaining acceptable structural performance. Pranoto et al., [25] compared ASTM A36 and JIS G3101 frame materials under impact loading, while Sabtu et al., [26] investigated stress distribution in AL6061-T6 frame structures under different applied loads [25,26]. These studies support the use of von Mises stress, displacement, equivalent strain, and FoS as important structural indicators in preliminary frame evaluation. For the present dynamometer design, FEA provides a systematic basis for assessing structural adequacy, identifying high-stress regions, estimating deformation response, and selecting a material-efficient configuration prior to prototype fabrication.

2.5 Operational Safety in Dynamometer Testing

Operational safety is another important requirement in motorcycle dynamometer design. During testing, the motorcycle is operated in a stationary but loaded condition, while the rear wheel, roller, drivetrain, and braking components may rotate at high speed. This creates several potential hazards, including entanglement, tire slippage, roller exposure, motorcycle instability, vibration, heat accumulation, and fire risk. Therefore, safety provisions should be considered during the design stage rather than added only after fabrication.

Doan et al., [13] highlighted that motorcycle dynamometer testing involves mechanical hazards associated with rotating components and vehicle restraint [13]. In addition, machine safety studies emphasize the importance of guarding, access restriction, and safe separation between operators and moving machinery [8,27]. For compact workshop-scale dynamometers, safety considerations may include stable frame construction, proper motorcycle positioning, wheel restraint, guarded rotating parts, adequate operator distance, emergency equipment, and clear monitoring of the test condition. These measures are essential to reduce risk during dynamometer operation and to ensure safe testing for both the operator and surrounding personnel.

Human monitoring is also relevant during dynamometer testing because operators need to observe real-time parameters such as speed, torque, power, temperature, and warning signals while remaining aware of mechanical and thermal hazards. Ioniță et al., (2025) emphasized that human-centered interface design should reduce cognitive overload through clear information presentation and visual legibility [28]. Related ergonomic studies also show that display position and visual working conditions can affect operator strain, workload, and situational awareness [29,30]. Although ergonomics is not the primary evaluation parameter in the present study, clear display visibility and safe operator positioning remain useful supporting considerations in the overall safety-oriented design of the dynamometer.

2.6 Research Gap

The reviewed literature indicates that research on motorcycle and small-vehicle dynamometers has predominantly focused on performance measurement, power and torque characterization, braking behavior, thermal effects, data acquisition, and the structural assessment of individual components. FEA has likewise been widely applied to evaluate frames, supports, and other load-bearing mechanical structures. Accordingly, the use of FEA alone does not constitute a methodological novelty. However, limited attention has been directed towards the systematic selection of compact eddy-current chassis dynamometer configurations specifically intended for motorcycles with engine capacities of up to 200cc, particularly where structural adequacy, controlled material reduction, and workshop-oriented operational safety are considered concurrently within a unified design framework. Previous studies have generally addressed structural strength, measurement capability, thermal behavior, and safety as separate design considerations rather than integrating them into a common design-selection procedure [24-26].

Existing motorcycle and small-vehicle chassis dynamometer studies also reflect different development objectives. Maniar et al. [16] investigated a portable 2-wheeler dynamometer test rig with emphasis on the performance of its associated control hardware, whereas Arifwardana et al. [15] employed a chassis dynamometer for the characterization of a hybrid 2-wheeler. Doan et al. [13] reported the development and manufacture of a motorcycle chassis dynamometer, demonstrating the practical implementation of a vehicle-level testing platform. In contrast, Bagaskoro and Aryadi [24] focused specifically on finite-element-based strength analysis of the rollers and supports of a

hydraulic chassis dynamometer. Collectively, these studies demonstrate the technical feasibility of motorcycle and small-vehicle dynamometer systems but primarily emphasize measurement capability, drivetrain characterization, fabrication, or the structural assessment of selected components.

The specific research gap addressed in the present study is therefore the limited integration of structural simulation outcomes with material-efficiency and operational-safety criteria during the preliminary design and selection of compact motorcycle dynamometers. Rather than selecting a configuration solely on the basis of minimum stress, minimum deformation, or maximum FoS, the proposed approach first establishes structural feasibility through mesh-verified static FEA and subsequently evaluates the feasible alternatives using material efficiency and operational safety criteria. 3 complete structural configurations are assessed under identical material, loading, boundary, and mesh conditions, allowing the structural consequences of progressively reducing the member thickness from 6.0mm to 5.0mm to be quantified directly while maintaining an explicit requirement for structural adequacy.

The structural results are subsequently integrated with material-efficiency and operational-safety considerations through a weighted multi-criteria design-selection framework. This approach enables a distinction between the most structurally conservative configuration and the one that provides a more balanced system-level compromise among structural margin, material utilization, and practical safety requirements. The principal contribution of the study, therefore, lies in the application-specific integration of structural assessment and preliminary design-selection criteria for a compact eddy-current chassis dynamometer intended for motorcycles up to 200cc.

The proposed system should not be interpreted as outperforming established commercial chassis dynamometers. Commercial systems generally incorporate mature control architectures, calibrated instrumentation, integrated cooling systems, comprehensive safety guarding, and validated operating procedures, none of which were experimentally benchmarked in the present study. Accordingly, the contribution of the proposed design is limited to its compact, application-specific structural development and preliminary multi-criteria evaluation. Therefore, no claim is made regarding superior measurement accuracy, braking capacity, durability, or overall operational performance relative to commercially available dynamometer systems.

3. Methodology

This study adopted a simulation-based comparative design approach to evaluate 3 eddy-current chassis dynamometer configurations for motorcycles with engine capacities up to 200cc. The methodology comprised 5 main stages, which are development of the design alternatives, definition of material properties and loading conditions, finite element modeling, mesh-convergence verification, and weighted multi-criteria design evaluation. SolidWorks Simulation 2025 was used to assess the von Mises stress, resultant displacement, equivalent strain, and FoS of each design under identical static loading and boundary conditions.

3.1 Research Workflow and Design Development

The overall research workflow is illustrated in Fig. 1. The process commenced with the development of 3-dimensional CAD models in SolidWorks. 3 design alternatives were created by systematically incorporating ergonomic, cooling, and safety enhancements while varying structural thickness. Each design was subjected to static structural FEA under identical loading and boundary

conditions. Simulation results for von Mises stress, displacement, strain, and FoS were compared, and a weighted evaluation method was used to determine the final design.

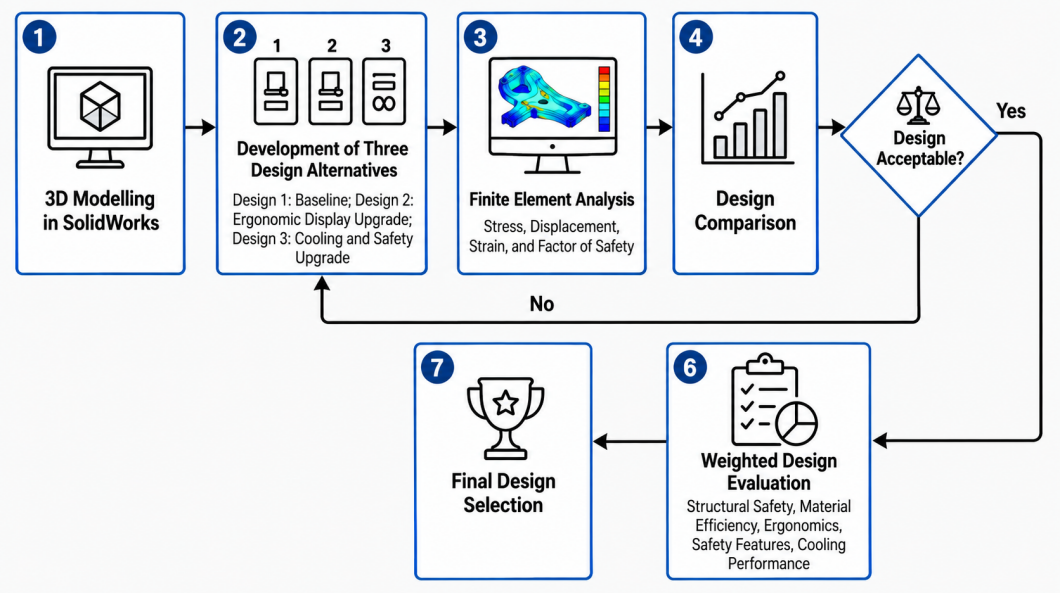


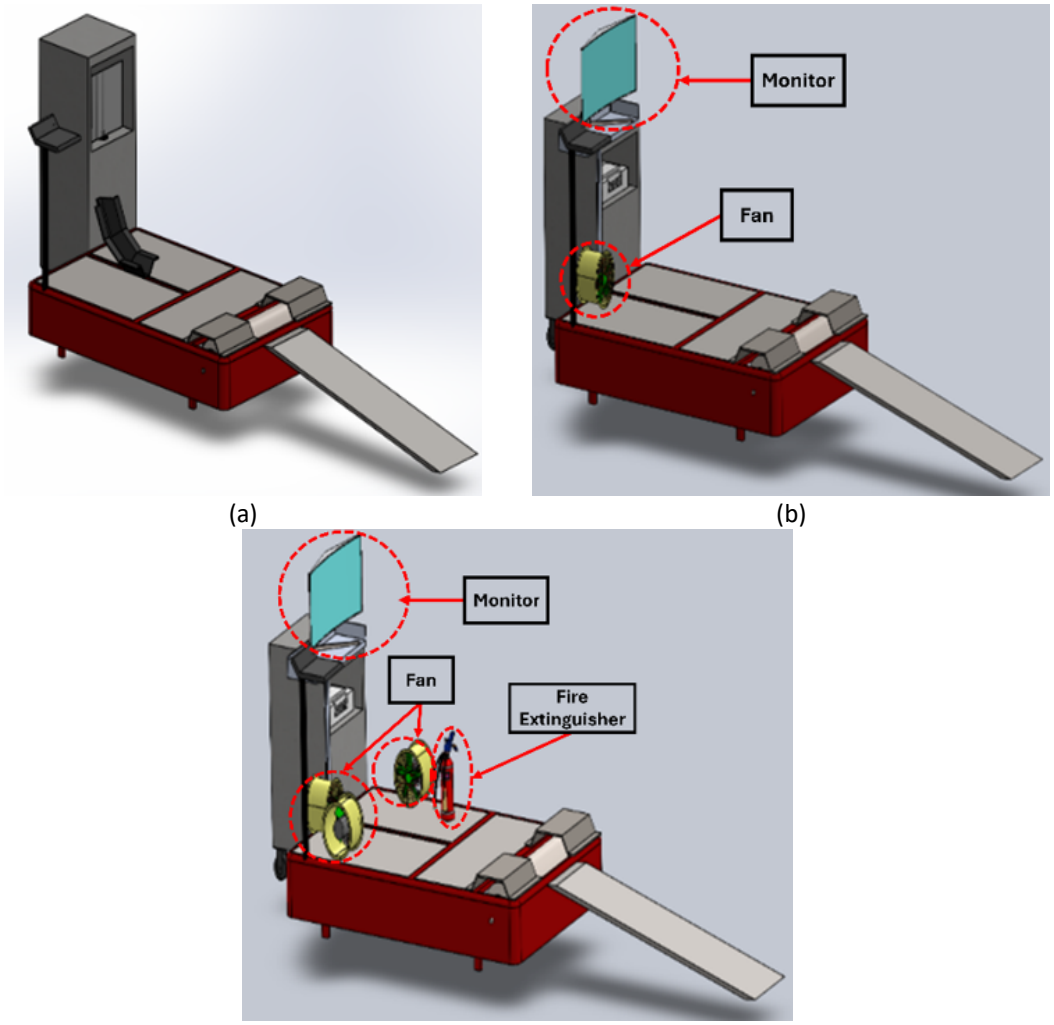
Fig. 1. Research workflow for the structural and safety-oriented optimization of the eddy-current chassis dynamometer.

Three (3) design configurations were developed using a systematic staged-progression approach. All configurations retained the same overall dynamometer architecture, comprising the main frame, motorcycle-supporting plate, roller-support region, and eddy-current brake mounting area. The configurations were therefore not conceived as independent geometries but as successive design iterations intended to isolate the effects of structural thickness reduction while progressively incorporating operational and safety considerations. The designs are presented in Figure 2.

Design 1 was established as the baseline configuration with a structural thickness of 6.0mm. This configuration served as the reference case for evaluating the effects of subsequent material reduction on structural performance. Design 2 represented the first material-efficiency iteration, in which the structural thickness was reduced by 0.5mm to 5.5mm. This intermediate configuration was introduced to determine whether a moderate reduction in structural thickness could be achieved while maintaining a response comparable to that of the baseline design.

Design 3 represented the second material-reduction iteration, with the structural thickness further reduced by 0.5mm to 5.0mm. This configuration was used to assess the additional structural consequences associated with a greater reduction in section thickness. In addition, Design 3 incorporated the most complete set of operational-safety provisions among the 3 alternatives, thereby extending the comparison from purely structural performance towards a broader system-level design assessment.

The uniform thickness increment of 0.5mm was used to ensure a controlled and directly comparable reduction between successive configurations, thereby allowing the structural consequences of progressive material reduction to be evaluated under otherwise identical simulation conditions. The main features and intended improvements of the 3 designs are summarized in Table 1.



(a) (b)

(c)

Fig. 2. Three (3) proposed eddy-current chassis dynamometer design alternatives: (a) Design 1 (baseline), (b) Design 2, and (c) Design 3.

Table 1
Summary of the proposed dynamometer design alternatives

Design	Structural Thickness	Design Role	Primary Development Objective	Operational Provision
1	6.0mm	Baseline configuration	Establish reference structural response	Basic configuration
2	5.5mm	First design iteration	Evaluate moderate material reduction while maintaining comparable structural and performance	Monitor and cooling provision
3	5.0mm	Second design iteration	Evaluate greater material reduction and integrate additional workshop-safety considerations	Monitor, cooling provision, and fire-extinguisher provision

3.2 Finite Element Analysis (FEA) Setup

The 3 design models were analyzed using SolidWorks Simulation 2025 under identical loading and boundary conditions. Plain carbon steel was selected for the primary structural components because the dynamometer was intended as a compact and workshop-scale testing system. The material was

selected based on its widespread availability, good weldability, ease of cutting and fabrication, compatibility with conventional workshop manufacturing processes, and sufficient yield strength for the preliminary loading condition considered in this study. The objective was not to minimize structural mass by using high-specific-strength materials, but rather to investigate whether material use could be reduced through controlled section-thickness reduction while maintaining adequate structural performance.

Alternative materials, including aluminium alloys and corrosion-resistant steels, could offer advantages in terms of specific strength, structural mass, or corrosion resistance. However, their adoption would introduce additional considerations related to stiffness, joining methods, fabrication requirements, and cost, which were beyond the scope of the present investigation. Plain carbon steel was therefore retained as a consistent baseline material to enable direct comparison among the 3 structural configurations without introducing material-dependent variables. Future work may extend the proposed framework through a systematic multi-material assessment incorporating structural performance, mass, cost, manufacturability, and corrosion resistance as concurrent design criteria. The material was also assumed to be homogeneous, isotropic, and linearly elastic under the applied static loading condition. The mechanical properties assigned in SolidWorks Simulation are presented in Table 2.

Table 2
Mechanical properties assigned to the structural material

Property	Value
Material	Plain carbon steel
Mass Density	$7800 kg/m^3$
Elastic Modulus	$2.1 \times 10^{11} N/m^2$
Poisson's Ratio	0.28
Shear Modulus	$7.9 \times 10^{10} N/m^2$
Yield Strength	220.6MPa
Tensile Strength	399.8MPa

A uniformly distributed vertical load of 1400N was applied to the motorcycle-supporting plate surface. The applied load corresponds to an assumed motorcycle mass of approximately 143kg, calculated using the gravitational acceleration of 9.81 m/s². This loading condition was selected to represent the static weight of a motorcycle with an engine capacity of up to 200cc supported by the dynamometer structure.

The load was distributed over the motorcycle-supporting plate to provide a simplified representation of the load transferred from the motorcycle to the dynamometer frame. Gravity was also included in the simulation to account for the self-weight of the structural components. Fixed supports were applied at the base mounting regions to represent the rigid attachment of the dynamometer frame to the workshop floor. The connected structural members were defined using bonded contacts to represent welded or rigidly connected joints.

The applied vertical load of 1400N was used as a preliminary static screening condition, corresponding to an equivalent motorcycle mass of 143kg under gravitational loading. This load was selected primarily to provide a consistent reference condition for comparing the 3 structural configurations rather than to reproduce the complete loading environment experienced during dynamometer operation. By maintaining identical material properties, support conditions, contact assumptions, and applied loading across all configurations, variations in the predicted structural

responses could be attributed primarily to the design modifications introduced, particularly the progressive reduction in structural thickness.

The present finite element model does not account for several operational loads that may influence the structural behavior of the dynamometer, including rider weight, dynamic tire-roller interaction forces, braking-torque reactions, vibration, transient or impact loading, fatigue, and thermal effects. These loading mechanisms may alter both the magnitude and spatial distribution of stresses during actual dynamometer operation. Accordingly, the predicted von Mises stress, displacement, strain, and FoS should be interpreted as comparative indicators under the prescribed static loading condition rather than as direct validation of operational structural safety. Further assessment incorporating representative operational load cases, dynamic and fatigue effects, and experimental measurements is therefore required before the selected configuration can be considered structurally validated for further prototype development and experimental validation. The main simulation conditions are summarized in Table 3.

Table 3
Finite element simulation setup

Parameter	Setting
Software	SolidWorks Simulation 2025
Analysis Type	Static structural analysis
Material	Plain carbon steel
Yield Strength	220.6MPa
Applied Load	1400N
Load Type	Uniformly distributed vertical load
Load Location	Motorcycle-supporting plate surface
Gravity	$9.81 m/s^2$
Boundary Condition	Fixed support at base mounting regions
Contact Condition	Bonded contacts
Structural Assumption	Linear elastic behavior
Analysis Outputs	von Mises stress, resultant displacement, equivalent strain, and FoS

3.3 Meshing and Mesh Verification

The finite element models were discretized using a 3-dimensional solid mesh in SolidWorks Simulation. A blended curvature-based mesher was selected because it is suitable for assemblies containing curved surfaces, geometric transitions, joints, and mounting regions. This mesher automatically refines the elements in geometrically complex regions while maintaining larger elements in less critical areas, thereby improving computational efficiency without compromising the representation of the model geometry [31,32]. High-quality second-order solid elements were used to improve the accuracy of the calculated stress and displacement responses.

The final mesh used a maximum element size of 132.99mm and a minimum element size of 9.567mm. The generated mesh consisted of 35,146 nodes and 18,386 elements. No distorted elements were reported, although the maximum element aspect ratio was 714.65. The mesh settings used in the final analysis are summarized in Table 4.

Although no distorted elements were detected, the final mesh recorded a relatively high maximum aspect ratio of 714.65. This value suggests the presence of highly elongated elements in localized geometric regions. Therefore, the mesh-quality result was interpreted together with the mesh-convergence analysis rather than relying solely on the maximum aspect ratio. The convergence

behaviour of the maximum von Mises stress and displacement was examined to determine whether these localized elements significantly influenced the overall structural results.

Table 4
Final finite element mesh settings

Parameter	Setting
Mesh Type	Solid mesh
Mesher Used	Blended curvature-based mesher
Element Order	High-quality second-order elements
Maximum Element Size	132.99mm
Minimum Element Size	9.567mm
Total Nodes	35,146
Total Elements	18,386
Maximum Aspect Ratio	714.65
Distorted Elements	0%

Although no distorted elements were detected, the final mesh recorded a relatively high maximum aspect ratio of 714.65. This value suggests the presence of highly elongated elements in localized geometric regions. Therefore, the mesh-quality result was interpreted together with the mesh-convergence analysis rather than relying solely on the maximum aspect ratio. The convergence behaviour of the maximum von Mises stress and displacement was examined to determine whether these localized elements significantly influenced the overall structural results.

A mesh convergence study was conducted using Design 1 as the baseline model to determine whether the simulation results were significantly affected by the selected element size. 4 mesh densities, namely coarse, medium, fine, and extra fine, were evaluated. The maximum von Mises stress and maximum resultant displacement were selected as the convergence parameters, consistent with their application in the finite element verification of structural frames [26]. The mesh convergence results are presented in Table 5.

Table 5
Mesh convergence results for Design 1

Mesh Setting	Maximum Element Size (mm)	Nodes	Elements	Maximum von Mises Stress (MPa)	Maximum Displacement (mm)	Stress Difference (%)
Coarse	166.64	30,664	15,720	54.69	0.7727	–
Medium	132.99	35,146	18,386	52.80	0.8680	3.46
Fine	106.66	36,510	19,006	53.95	0.8918	2.18
Extra Fine	93.32	37,778	19,593	53.44	0.9110	0.95

The variation in maximum von Mises stress decreased progressively as the mesh was refined. The stress difference was 3.46% between the coarse and medium meshes, 2.18% between the medium and fine meshes, and 0.95% between the fine and extra-fine meshes. The maximum displacement also showed a converging trend, increasing from 0.7727mm for the coarse mesh to 0.9110mm for the extra-fine mesh.

Compared with the extra-fine mesh, the medium mesh produced differences of approximately 1.20% in maximum von Mises stress and 4.72% in maximum displacement. Since both differences were below the adopted convergence criterion of 5%, the medium mesh was selected for the final structural analysis. This mesh provided an appropriate balance between computational efficiency and numerical accuracy. The same meshing procedure was subsequently applied to all 3 design configurations to ensure a consistent comparison of their structural performance.

3.4 Structural Performance Parameters

The structural performance of each design was evaluated based on the maximum von Mises stress, maximum resultant displacement, maximum equivalent strain, and minimum FoS. The maximum von Mises stress was compared with the yield strength of the assigned plain carbon steel to determine whether yielding was predicted under the applied static loading condition. Resultant displacement was used to assess the stiffness and deformation response of the dynamometer structure, while equivalent strain was used to characterize the local deformation response.

The FoS values were obtained directly from SolidWorks Simulation based on the assigned material yield strength and the calculated maximum von Mises stress. For verification and interpretation, the FoS is expressed using Eq. (1):

$$FoS = \frac{\sigma_y}{\sigma_{v,max}} \quad \text{(Eq. 1)}$$

Where *FoS* is the Factor of Safety, σ_y is the material yield strength, and $\sigma_{v,max}$ is the maximum von Mises stress obtained from the simulation. A FoS greater than 1.0 indicates only that the predicted maximum von Mises stress remains below the assigned material yield strength under the prescribed static loading condition. This threshold alone was considered insufficient for preliminary structural screening. Accordingly, a minimum FoS of 2.0 was adopted to provide an additional design margin against uncertainties associated with material properties, idealized loading and boundary conditions, welded connections, and fabrication variability. The selected value is therefore used as a study-specific preliminary screening criterion and should not be interpreted as evidence of compliance with any particular design code, certification requirement, or operational safety standard. Stress utilization was calculated to determine the percentage of the material yield strength utilized by each design, as expressed in Eq. (2):

$$Stress\ utilisation\ (\%) = \frac{\sigma_{v,max}}{\sigma_y}\ X\ 100 \quad \text{(Eq. 2)}$$

A lower stress utilization value indicates a more conservative structural response and a larger remaining safety margin. In contrast, a higher value indicates greater utilization of the material strength but a lower safety margin. Stress utilization was therefore interpreted together with the FoS, displacement, and equivalent strain when comparing the 3 designs.

3.5 Weighted Design Evaluation

A weighted multi-criteria evaluation was used to select the most suitable design by combining the structural simulation results with practical design considerations. The evaluation criteria consisted of structural safety, material efficiency, and operational safety readiness. Structural safety was assessed using the minimum FoS obtained from FEA. Material efficiency was evaluated based on the reduction in structural thickness relative to the baseline design. Operational safety readiness was assessed by the inclusion of safety-related provisions in workshop operations.

Each criterion was assigned a weighting factor, and each design was rated using a 5-point scale, where a rating of 1 represented very poor performance and a rating of 5 represented excellent performance. The total weighted score for each design was calculated using:

$$S_j = \sum_{i=1}^{n} W_i R_{i,j} \quad \text{(Eq. 3)}$$

where S_j is the total weighted score, W_i is the weighting factor for each criterion, and $R_{i,j}$ is the rating assigned to each design. The design with the highest total weighted score was selected as the preferred configuration. The evaluation criteria and their assigned weightings are presented in Table 6.

Table 6
Weighted evaluation criteria

Criteria	Evaluation Basis	Weight (%)
Structural Safety	Minimum factors of safety from FEA	40
Material Efficiency	Thickness reduction relative to baseline	35
Operational Safety Readiness	Safety-related provisions for workshop operation	25
Total		100

The weighting distribution placed the greatest emphasis on structural safety, followed by material efficiency and operational safety readiness. This distribution was selected because adequate structural strength is the primary requirement of the dynamometer frame, while material reduction and practical safety provisions are also important for compact workshop-scale operation.

4. Results and Discussion

This section presents the finite element simulation results for the 3 proposed eddy-current chassis dynamometer designs under a uniformly distributed static load of 1400N. The designs were evaluated based on von Mises stress, resultant displacement, equivalent strain, and minimum FoS These parameters were used to assess structural adequacy, deformation response, elastic behaviour, and safety margin. The results were then integrated with material-efficiency and operational-safety considerations to support the preliminary selection of the most suitable design.

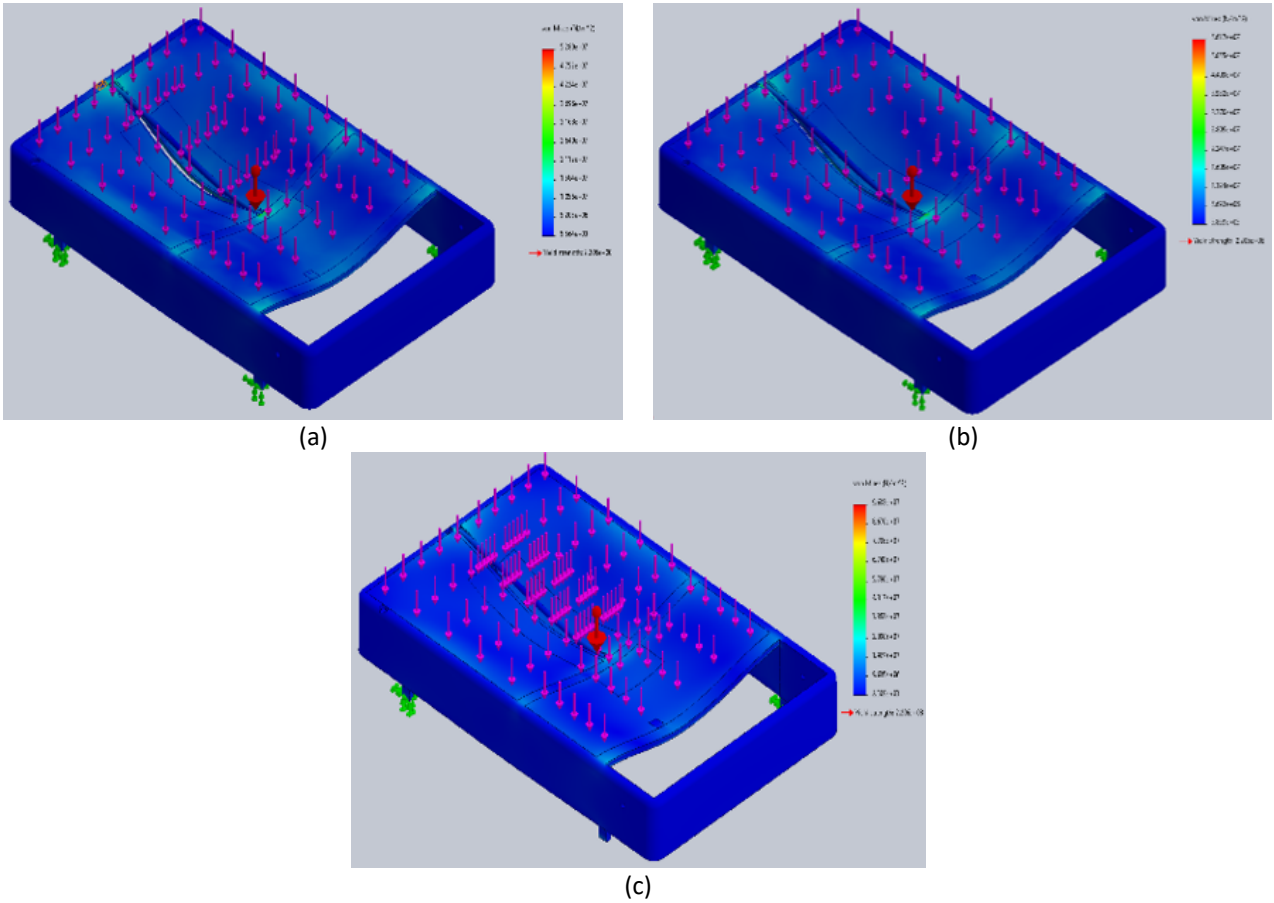
4.1 Von Mises Stress Analysis

Fig. 3 presents the von Mises stress distributions for the 3 dynamometer designs under the applied static load of 1400N. For all configurations, the highest stress occurred primarily in the central region of the motorcycle-supporting plate. This distribution indicates that the structural response was dominated by bending of the loaded plate and the transfer of load toward the surrounding frame members.

The maximum von Mises stress values and stress utilization are summarized in Table 7. Relative to Design 1, the maximum stress increased by 6.38% for Design 2 and 82.44% for Design 3. The relatively small increase observed for Design 2 indicates that reducing the structural thickness from 6.0mm to 5.5mm produced only a limited change in the predicted stress response. In contrast, the further reduction to 5.0mm in Design 3 resulted in a substantially higher stress level. This increase was primarily associated with the lower bending stiffness of the thinner structure and may also have been influenced by local geometric differences between the design configurations.

However, the maximum stresses for all 3 designs remained below the assigned yield strength of plain carbon steel, 220.6MPa. The corresponding stress utilization values were 23.90%, 25.50%, and

43.70% for Design 1, Design 2, and Design 3, respectively. Design 1, therefore, exhibited the most conservative stress response, while Design 3 utilized a greater proportion of the available material strength. These results indicate that yielding was not predicted for any design under the specified static loading condition.



(a) (b) (c)

Fig. 3 Von Mises stress distribution: (a) Design 1, (b) Design 2, and (c) Design 3.

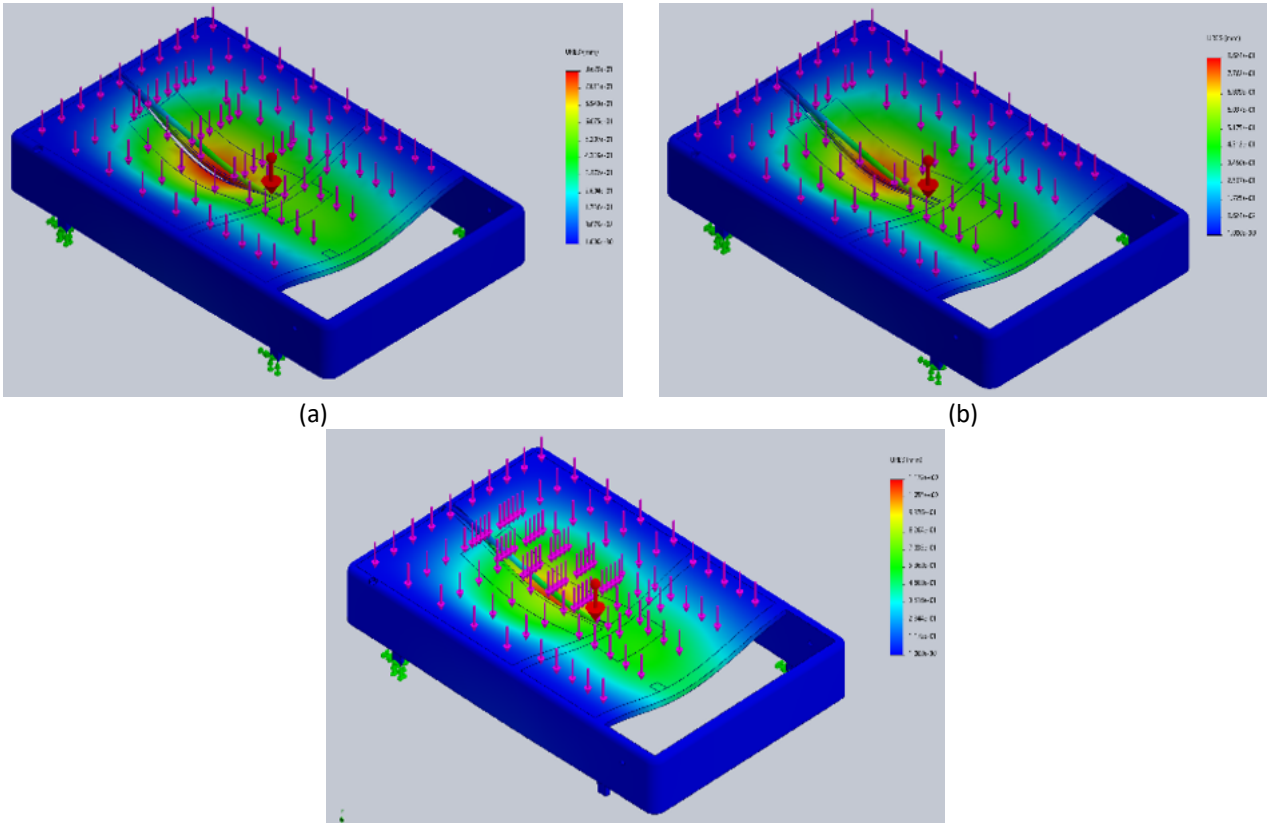
Table 7
Von Mises stress comparison of the 3 designs

Design	Thickness (mm)	Maximum Stress (MPa)	Stress Utilization (% of 220.6 MPa yield)
1	6.0	52.80	23.90
2	5.5	56.17	25.50
3	5.0	96.33	43.70

The observed increase in stress with reduced structural thickness is consistent with the general behavior reported in previous finite element studies of dynamometer supports and frame structures [24-26]. However, direct numerical comparison is limited because of differences in geometry, material properties, loading conditions, and boundary assumptions. Therefore, the present findings should be interpreted as a comparative assessment of the 3 proposed designs rather than confirmation of their performance under actual operating conditions.

4.2 Displacement Analysis

Fig. 4 presents the resultant displacement distributions for the 3 dynamometer designs. In all configurations, the maximum displacement occurred near the central region of the motorcycle-supporting plate, corresponding to the location of the applied vertical load. This pattern is consistent with the von Mises stress distributions and indicates that the structural response was primarily governed by bending of the loaded plate.



(a) (b)

(c)

Fig. 4. Resultant displacement distribution: (a) Design 1, (b) Design 2, and (c) Design 3.

The maximum resultant displacement values are summarised in Table 8. Design 2 recorded the lowest displacement of 0.862mm, followed closely by Design 1 at 0.868mm. Design 3 produced the highest displacement of 1.172mm. The difference between Design 1 and Design 2 was only 0.006mm, equivalent to approximately 0.69%. This difference was smaller than the displacement variation observed during the mesh-convergence study and was therefore considered numerically negligible. Consequently, Design 1 and Design 2 exhibited comparable global deformation responses under the applied static load, indicating no meaningful improvement in the stiffness of Design 2.

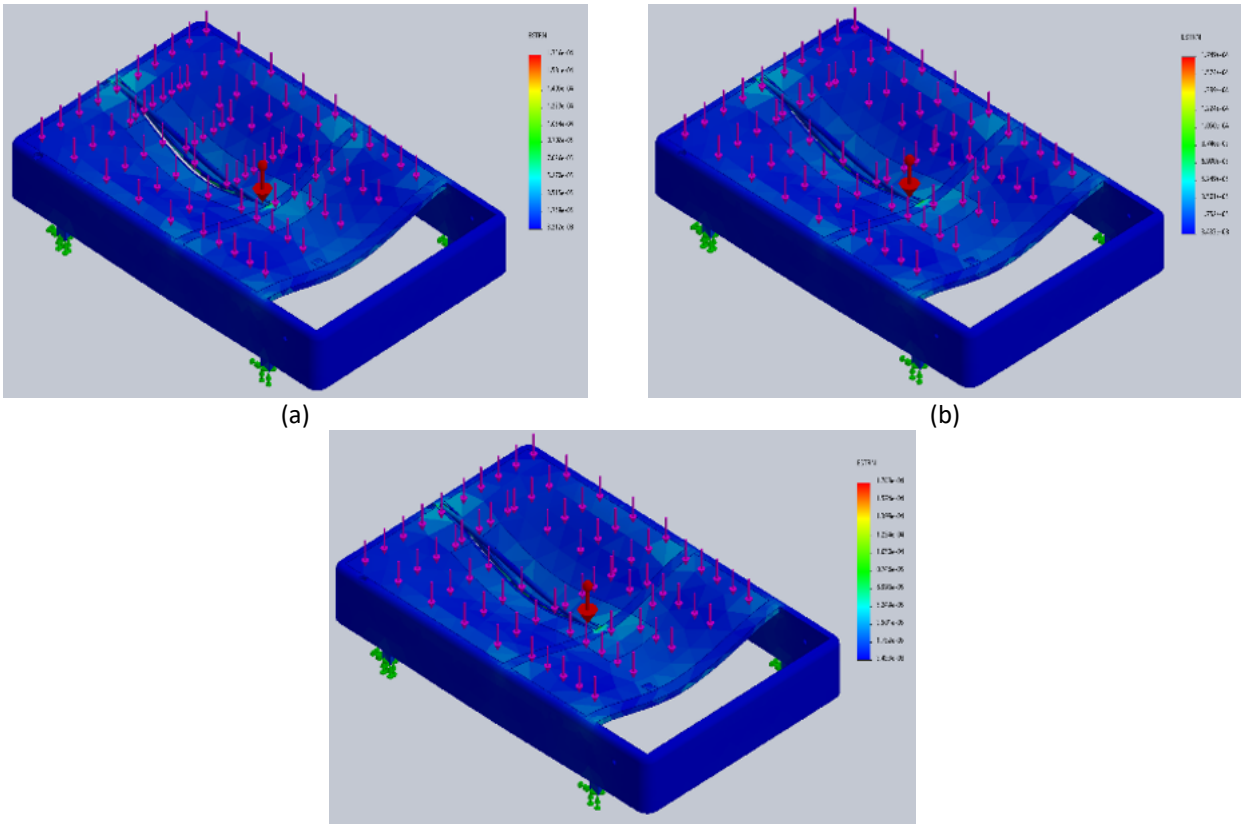
Table 8
Displacement comparison of the 3 designs

Design	Thickness (mm)	Maximum Displacement (mm)
1	6.0	0.868
2	5.5	0.862
3	5.0	1.172

In contrast, Design 3 recorded a displacement approximately 35.02% higher than Design 1. This increase was consistent with the reduced structural thickness of 5.0mm, which lowered the bending stiffness of the motorcycle-supporting plate. Local geometric differences in Design 3 may also have contributed to its greater deformation response. Although the maximum displacement for all designs remained below 1.2mm, no specific allowable-deflection criterion was established in this study. Therefore, these values should not be interpreted as direct confirmation of acceptable operational rigidity. Further dynamic and experimental assessments are required to determine whether the predicted deformation affects roller alignment, tire-roller contact, vibration response, and measurement repeatability during actual dynamometer operation.

4.3 Equivalent Strain Analysis

Fig. 5 presents the equivalent strain distributions for the 3 dynamometer designs. Across all configurations, the highest strain was concentrated in the central region of the motorcycle-supporting plate, corresponding to locations of higher von Mises stress and resultant displacement. This distribution indicates that the strain response was primarily governed by bending deformation under the applied vertical load.



(a) (b)

(c)

Fig. 5. Equivalent strain distribution: (a) Design 1, (b) Design 2, and (c) Design 3.

The maximum equivalent strain values obtained for the 3 designs are presented in Table 9. Design 3 recorded the highest equivalent strain, consistent with its reduced structural thickness and greater stress and displacement responses. Design 1 and Design 2 exhibited lower and relatively comparable strain levels, indicating similar elastic deformation behavior under the specified static loading condition.

Table 9
Equivalent strain comparison of the 3 designs

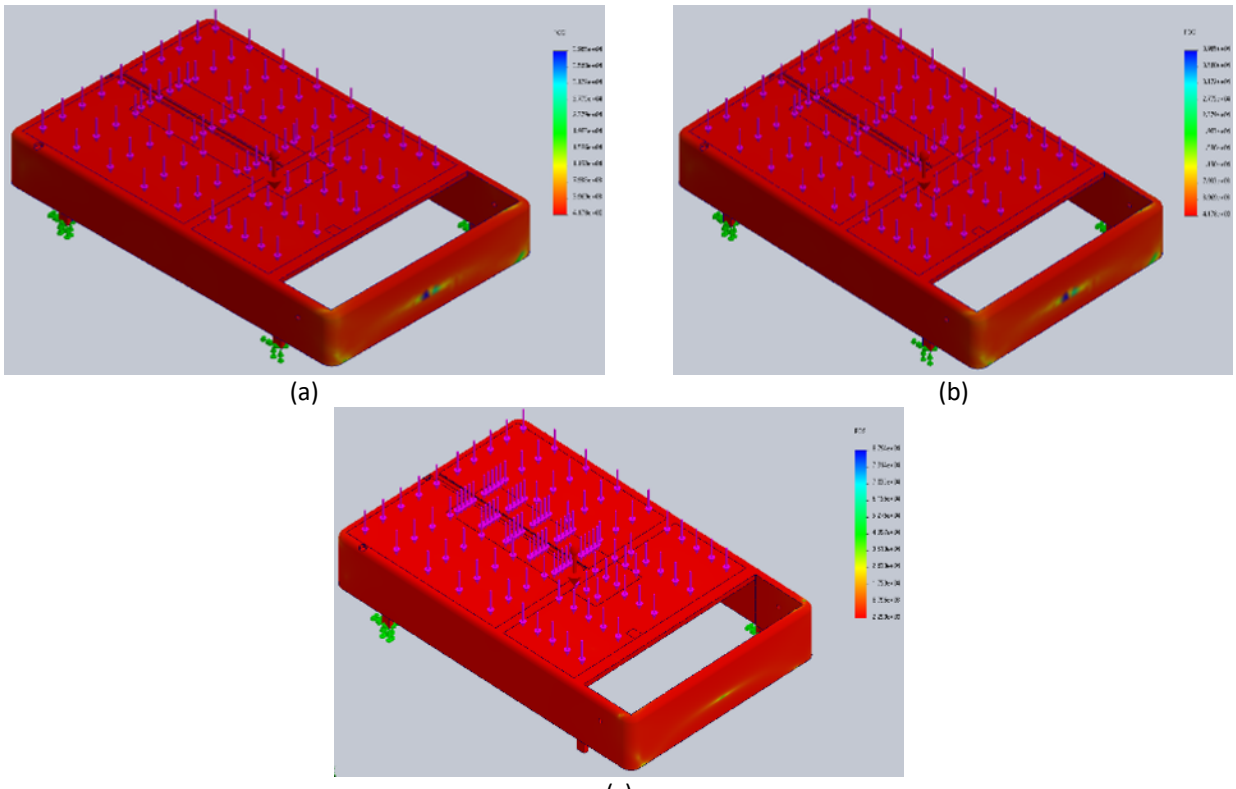
Design	Thickness (mm)	Maximum Equivalent Strain
1	6.0	1.756×10^{-4}
2	5.5	1.749×10^{-4}
3	5.0	3.208×10^{-4}

The equivalent strain results followed the general trend observed in the stress analysis, with a reduction in structural thickness increasing the local deformation response. However, the maximum von Mises stresses for all 3 designs remained below the assigned material yield strength. Under the linear-elastic material assumption adopted in the simulation, this indicates that permanent deformation was not predicted under the applied static load.

The strain distribution should be interpreted together with the von Mises stress, displacement, and FoS results. Although Design 3 experienced the highest equivalent strain, its structural response remained within the modeled elastic range. However, further experimental and dynamic analyses are required to confirm the strain behavior under actual dynamometer operating conditions, particularly in the presence of vibration, braking torque reaction, fatigue loading, and tire-roller interaction.

4.4 Factor of Safety (FoS) Analysis

Fig. 6 presents the FoS distributions for the 3 dynamometer designs. The minimum FoS occurred within the higher-stress regions of the motorcycle-supporting plate, corresponding to the locations identified in the von Mises stress analysis. As expected, regions subjected to higher stress produced lower FoS values.



(a) (b)

(c)

Fig. 6. FoS distribution: (a) Design 1, (b) Design 2, and (c) Design 3.

The FoS generally decreased as structural thickness decreased. Design 2 showed only a moderate reduction of approximately 7.14% relative to Design 1, indicating that decreasing the thickness from 6.0mm to 5.5mm produced a limited reduction in the structural safety margin. In contrast, Design 3 recorded a FoS approximately 45.24% lower than Design 1, consistent with its higher maximum von Mises stress and reduced structural thickness.

All 3 configurations exceeded the adopted preliminary FoS screening criterion of 2.0 under the specified static loading condition, with minimum values of 4.2, 3.9, and 2.3 for Design 1, Design 2, and Design 3, respectively. Design 1 provided the greatest structural safety margin, while Design 2 maintained a relatively high margin despite the moderate reduction in thickness. Although Design 3 provided the lowest safety margin, its minimum FoS of 2.3 remained above the adopted preliminary screening criterion of 2.0. Therefore, Design 3 may be considered structurally feasible for preliminary development, but it provides less tolerance for uncertainties in loading, material properties, welded joints, fabrication quality, and boundary conditions.

The FoS results confirm that yielding was not predicted for any of the designs under the applied static load. However, these values should not be interpreted as confirmation of operational safety, as the analysis excluded dynamic loading, braking-torque reaction, vibration, fatigue, thermal effects, weld imperfections, and tire-roller interaction. Further prototype testing and operational validation are therefore required before the selected design is used under actual dynamometer testing conditions.

Table 10
FoS comparison of the 3 designs

Design	Thickness (mm)	Minimum FoS
1	6.0	4.2
2	5.5	3.9
3	5.0	2.3

The FoS results confirm that yielding was not predicted for any of the designs under the applied static load. However, these values should not be interpreted as confirmation of operational safety, as the analysis excluded dynamic loading, braking-torque reaction, vibration, fatigue, thermal effects, weld imperfections, and tire-roller interaction. Further prototype testing and operational validation are therefore required before the selected design is used under actual dynamometer testing conditions.

4.5 Overall Structural Performance Comparison

The overall structural performance of the 3 designs is summarised in Table 11. Relative to the 6.0mm baseline configuration, the structural thickness was reduced by 8.33% for Design 2 and 16.67% for Design 3. The reduction in thickness generally increased the maximum von Mises stress and reduced the FoS. However, the displacement responses of Design 1 and Design 2 remained comparable, whereas Design 3 exhibited a more pronounced increase in deformation.

Design 1 demonstrated the most conservative structural response, with the lowest maximum stress, lowest stress utilization, and highest FoS. Its structural performance provided the largest safety margin under the applied static load, although the low stress utilization indicated potential for reducing the structural thickness. Design 2 achieved a more balanced structural response. Compared with Design 1, its maximum stress increased by only 6.38%, while its displacement remained essentially unchanged and its FoS remained high at 3.9. Therefore, Design 2 provided the strongest

balance between thickness reduction and structural performance when only the finite element results were considered. Design 3 achieved the greatest thickness reduction but recorded the highest stress and displacement.

Table 11
Overall structural performance comparison

Parameter	Design 1	Design 2	Design 3
Structure Thickness (mm)	6.0	5.5	5.0
Maximum von Mises Stress (Mpa)	52.80	56.17	96.33
Stress Utilization (% Of Yield Strength)	23.90	25.50	43.70
Maximum Displacement (mm)	0.868	0.862	1.172
Maximum Equivalent Strain	1.756×10^{-4}	1.749×10^{-4}	3.208×10^{-4}
Minimum Fos	4.2	3.9	2.3

Relative to Design 1, its maximum stress increased by 82.44%, while its displacement increased by 35.02%. However, its maximum stress remained below the material yield strength, and its FoS of 2.3 exceeded the adopted preliminary criterion of 2.0. Design 3 was therefore considered structurally feasible for preliminary development and satisfied the adopted static screening criterion, although it provided the smallest safety margin among the 3 configurations. Design 3 was therefore retained as a candidate for further development. However, its structural adequacy under representative operational loading remains to be verified.

Overall, under the specified 1400N static vertical loading condition, all 3 configurations exceeded the adopted preliminary FoS screening criterion of 2.0. Design 1 offered the greatest structural safety margin, Design 2 provided the most balanced structural configuration, and Design 3 achieved the greatest thickness reduction while maintaining the minimum required FoS. Since material efficiency was assessed based on structural thickness rather than total CAD mass or material volume, the results represent a relative thickness reduction and should not be interpreted directly as confirmed weight or fabrication cost savings. The final design selection was therefore supported by the weighted evaluation of structural safety, material efficiency, and operational safety readiness presented in the following section.

4.6 Safety-Oriented Design Evaluation

A weighted multi-criteria evaluation was conducted to integrate the structural simulation results with material-efficiency and operational-safety considerations. The evaluation criteria and weighting factors were defined in Table 6, with structural safety assigned the highest weight of 0.40, followed by material efficiency at 0.35 and operational safety readiness at 0.25. Each design was rated using a 5-point scale, and the weighted evaluation results are presented in Table 12.

Table 12
Weighted design evaluation

Criteria	Weight	Design 1		Design 2		Design 3	
		Rating	Score	Rating	Score	Rating	Score
Structural Safety	0.40	5	2.00	4	1.60	3	1.20
Material Efficiency	0.35	3	1.05	4	1.40	5	1.75
Operational Safety Readiness	0.25	1	0.25	2	0.50	5	1.25
Total Score	1.00		3.30		3.50		4.20

(5-point scale: 1 = very poor, 5 = excellent)

Design 1 received the highest structural-safety rating because it recorded the largest FoS of 4.2. However, its greater structural thickness and limited integration of operational safety provisions resulted in lower ratings for material efficiency and safety readiness. Consequently, Design 1 achieved a total weighted score of 3.30. Design 2 maintained a high FoS of 3.9 while reducing the structural thickness by 8.33% relative to the baseline design. Its comparable displacement response and moderate improvement in material efficiency resulted in a higher total score of 3.50. From a purely structural perspective, Design 2 represented the most balanced configuration. Design 3 received the lowest structural-safety rating because it recorded the smallest FoS of 2.3. However, it satisfied the adopted preliminary FoS criterion of 2.0 and achieved the greatest thickness reduction of 16.67%. In addition, the conceptual configuration incorporated more operational safety provisions than the other alternatives. These characteristics resulted in the highest total weighted score of 4.20.

The selection of Design 3 should be interpreted as the outcome of a multi-criteria trade-off rather than as evidence of superior structural performance. Relative to Design 1, Design 3 achieved a 16.67% reduction in structural thickness. However, this reduction was accompanied by an 82.44% increase in maximum von Mises stress and a 35.02% increase in maximum displacement, while the FoS decreased from 4.2 to 2.3. These changes quantify the structural penalty associated with the greater reduction in material usage. Nevertheless, Design 3 remained above the adopted preliminary FoS screening threshold of 2.0 under the prescribed static loading condition. Its higher overall weighted score, therefore, reflects the combined contributions of material efficiency and operational safety readiness, rather than superior structural performance in isolation.

In contrast, Design 2 provided the strongest compromise when only structural performance and thickness reduction were considered, because its stress increased by only 6.38% relative to Design 1, its displacement remained essentially unchanged, and its FoS remained high at 3.9. Accordingly, Design 2 may be preferable where structural robustness is prioritized, whereas Design 3 is preferred only under the broader weighting framework adopted in this study.

Based on the adopted weighting and rating framework, Design 3 was identified as the preferred preliminary configuration. However, this selection does not indicate that Design 3 provided the best structural performance. Instead, it reflects the best overall balance among structural adequacy, thickness reduction, and operational safety readiness within the criteria used in this study. The result should therefore be interpreted as a preliminary design decision and should be supported by sensitivity analysis, prototype fabrication, and experimental validation under representative operating conditions

4.7 Final Design Selection and Engineering Implications

Based on the weighted multi-criteria evaluation, Design 3 achieved the highest overall score of 4.20 and was selected as the preferred preliminary configuration. Although it recorded the highest maximum von Mises stress of 96.33MPa and the greatest displacement of 1.172mm, its stress remained below the assigned yield strength of 220.6MPa, while its minimum FoS of 2.3 exceeded the adopted preliminary criterion of 2.0. The selection of Design 3 reflects an engineering trade-off between structural safety and material utilization. Reducing the structural thickness from 6.0mm to 5.0mm increased stress and deformation and reduced the safety margin. However, the design achieved the greatest thickness reduction while maintaining acceptable performance under the specified static loading condition. Its higher weighted score was also supported by the inclusion of additional operational safety provisions.

Design 3 represents a more aggressive material-reduction strategy. Reducing the structural thickness from 6.0mm to 5.0mm decreased the nominal thickness by 16.67%, but increased the

maximum von Mises stress from 52.80MPa to 96.33MPa and the displacement from 0.868mm to 1.172 mm. Its FoS consequently decreased from 4.2 to 2.3. Thus, the material reduction produced a clear structural penalty. Despite this penalty, Design 3 remained above the adopted preliminary FoS screening criterion of 2.0 under the specified static load. Its higher overall weighted score resulted from a combination of greater material efficiency and more extensive operational safety provisions. Therefore, the preference for Design 3 is conditional on the adopted weighting framework and should not be interpreted as evidence that its structural disadvantages are negligible. Since no independent allowable-displacement criterion was established, the higher displacement of Design 3 cannot be considered operationally acceptable solely on the basis of the present static analysis. Its suitability, therefore, requires further verification under braking-torque reaction, vibration, tire-roller interaction, fatigue, and representative dynamic loading, followed by prototype testing.

The lower safety margin of Design 3 requires careful control of material quality, weld integrity, joint preparation, mounting accuracy, and frame alignment during fabrication. In addition, its structural performance should be verified under operational loading conditions, including roller rotation, braking-torque reaction, tire-roller interaction, vibration, fatigue, and thermal effects. Design 3 is recommended for further prototype development and experimental validation. Its final suitability for motorcycle dynamometer operation should be confirmed through dynamic analysis, sensitivity assessment of the weighted criteria, fabrication inspection, and testing under representative workshop conditions.

An important outcome of the proposed evaluation framework is that the configuration exhibiting the most favorable structural performance is not necessarily the preferred overall design. When structural response and thickness reduction were considered exclusively, Design 2 provided the most balanced compromise between structural safety margin and material reduction. However, once operational-safety readiness was incorporated into the evaluation, Design 3 emerged as the preferred preliminary configuration. This distinction highlights the importance of extending conventional stress-based structural optimization beyond purely structural criteria toward a broader system-level design evaluation. For compact chassis dynamometer applications, such an approach enables structural adequacy, material utilization, and operational safety to be considered concurrently, thereby supporting a more comprehensive preliminary design-selection process.

5. Conclusions

This study developed and evaluated 3 eddy-current chassis dynamometer designs for motorcycles with engine capacities of up to 200cc. The designs were analyzed using static FEA under a uniformly distributed vertical load of 1400N. Structural performance was assessed using von Mises stress, resultant displacement, equivalent strain, and FoS, while material efficiency and operational safety readiness were evaluated through a weighted multi-criteria evaluation.

All 3 configurations exhibited maximum von Mises stresses below the assigned yield strength of plain carbon steel, 220.6MPa, and satisfied the adopted preliminary FoS screening criterion of 2.0 under the prescribed 1400N static loading condition. Design 1 exhibited the lowest maximum von Mises stress of 52.80MPa and the highest FoS of 4.2, representing the most conservative structural configuration. Design 2 achieved an 8.33% reduction in structural thickness while maintaining a maximum von Mises stress of 56.17MPa, a resultant displacement of 0.862mm, and an FoS of 3.9. These results indicate that Design 2 provided the most balanced structural response among the 3 configurations, achieving material reduction without substantial deterioration in structural performance.

Design 3 achieved the greatest reduction in structural thickness, which is at 16.67%. However, this improvement was accompanied by the highest maximum von Mises stress of 96.33MPa, the greatest displacement of 1.172mm, and the lowest FoS of 2.3. Therefore, Design 3 did not exhibit the most favorable structural response when evaluated solely on the basis of stress, displacement, and FoS. Nonetheless, its maximum stress remained below the material yield strength, and its FoS remained above the adopted preliminary screening criterion of 2.0. In comparison, Design 2 retained a higher FoS of 3.9 and a displacement closer to that of the baseline configuration, making it the more balanced option from a purely structural perspective.

Despite its comparatively less favourable structural response, Design 3 achieved the highest weighted evaluation score of 4.20 and was identified as the preferred preliminary configuration. This outcome resulted from the adopted multi-criteria framework, which considered material efficiency and operational safety readiness in addition to structural adequacy. Accordingly, the selection of Design 3 reflects a system-level trade-off rather than structural superiority. Under the prescribed static loading condition, Design 3 remained within the adopted preliminary structural acceptance criteria while providing the greatest reduction in structural thickness and the highest operational-safety-readiness rating. However, this preference is dependent on the adopted weighting scheme and should not be interpreted as confirmation of superior structural strength or operational safety.

The findings of this study should therefore be regarded as a preliminary numerical assessment rather than a final validation of the proposed dynamometer design. The FEA considered only a simplified static vertical loading condition and did not account for several operating effects that may influence the structural response, including rider weight, roller rotation, tire-roller interaction, braking torque reaction, vibration, fatigue loading, weld imperfections, and thermal effects. In addition, the structural response, manufacturability, operational safety, and practical feasibility of Design 3 have not yet been experimentally verified.

Consequently, further development should include dynamic and fatigue analyses, sensitivity assessment of the weighting criteria, prototype fabrication, dimensional and weld-quality inspection, controlled static load testing, strain and displacement measurements, vibration assessment, braking-torque loading, tire-roller interaction testing, and evaluation under representative motorcycle operating conditions. Correlation between experimentally measured responses and finite element predictions will be essential for assessing the accuracy of the numerical model and identifying discrepancies arising from modeling assumptions, fabrication tolerances, joint behavior, and actual loading conditions. Until satisfactory numerical-experimental correlation and representative operational testing have been completed, Design 3 should be regarded as a candidate for further development rather than a fully validated operational dynamometer design.

Acknowledgement
This research was supported by Universiti Tun Hussein Onn Malaysia (UTHM) through Tier 1 (Vot No. J117).

Conflict of Interest Statement
The authors declare that there is no conflict of interest regarding the publication of this paper. No financial support, grants, or other forms of compensation were received that could have influenced the outcomes of this work. The research was conducted in the absence of any commercial or financial relationships that could be construed as a potential conflict of interest.

Author Contributions Statement

Mohd Mustaqim Tukiman contributed to the conceptualization, methodology, investigation, formal analysis, data curation, validation, supervision, project administration, preparation of the original draft, and review and editing of the manuscript; Aida Husna Ahmad contributed to the conceptualization, formal analysis, data curation, preparation of the original draft; Mohd Firdaus Abas contributed to the simulation, investigation, data collection, formal analysis, validation, data interpretation, and review and editing; Eliza M. Yusup contributed to data interpretation and review and editing; and Shahrul Azmir Osman contributed to the conceptualization, methodology, validation, supervision, project administration, and review and editing. All authors read and approved the final version of the manuscript.

Data Availability Statement

All data generated or analysed during this study are included in this published article. Additional datasets are available from the corresponding author upon reasonable request. Where applicable, publicly available datasets used in the study are cited in the references.

Ethics Statement

This study was conducted in accordance with the ethical standards of the institutional and/or national research committee. Ethical approval was obtained where required, and informed consent was obtained from all participants involved in the research.

References

[1] Khalaf I. Hamada And M. M. Rahman, "An Experimental Study For Performance And Emissions Of A Small Four-Stroke SI Engine For Modern Motorcycle," *International Journal Of Automotive And Mechanical Engineering*, Vol. 10, Pp. 1852–1865, Dec. 2022, doi: 10.15282/ijame.10.2014.3.0154.

[2] S. Mahesh, G. Ramadurai, And S. M. Shiva Nagendra, "Real-World Emissions Of Gaseous Pollutants From Motorcycles On Indian Urban Arterials," *Transp. Res. D Transp. Environ.*, Vol. 76, Pp. 72–84, Nov. 2019, doi: 10.1016/j.trd.2019.09.010.

[3] P. Pokharel, J. Espinoza, A. Pencheon, And D. Pleasant, "Development And Testing Of An Engine Dynamometer For Formula Style Engines," In *Volume 7: Engineering Education; Fluids Engineering*, American Society Of Mechanical Engineers, Nov. 2025. doi: 10.1115/IMECE2025-165166.

[4] İ. Uluocak And H. Yavuz, "Artificial Intelligence Based PID Controller For An Eddy Current Dynamometer," *Intelligent Automation & Soft Computing*, Vol. 33, No. 2, Pp. 1229–1243, 2022, doi: 10.32604/iasc.2022.023835.

[5] H. Hassanpour, S. Ebrahimi-Nejad, And M. Mollajafari, "Parametric Study Of Permanent Magnet Eddy Current Brake Considering Demagnetization, Temperature, Edge, And Skin Effects: Numerical And Experimental Investigation," *Applications In Engineering Science*, Vol. 22, P. 100235, Jun. 2025, doi: 10.1016/j.apples.2025.100235.

[6] K. Zhang, H. Shang, J. Xu, J. Niu, And Y. Yue, "Testing And Performance Analysis Of An Integrated Electromagnetic And Hydraulic Retarder For Heavy-Duty Vehicles," *Eng. Appl. Artif. Intell.*, Vol. 126, P. 106906, Nov. 2023, doi: 10.1016/j.engappai.2023.106906.

[7] S. Zhang, J. Wang, Z. Mu, Y. Zhang, And P. Yang, "Research On Water Cooling Control Strategies And Factors Influencing Disc-Type Eddy Current Brakes," *Case Studies In Thermal Engineering*, Vol. 75, P. 107089, Nov. 2025, doi: 10.1016/j.csite.2025.107089.

[8] M. Alhanouti And F. Gauterin, "Thorough Analysis Of The Reliability Of Measurements On Chassis Roller Dynamometer And Accurate Energy Consumption Estimation For Electric Vehicles," *Energies (Basel).*, Vol. 16, No. 24, P. 7994, Dec. 2023, doi: 10.3390/en16247994.

[9] R. J. Simonson, J. R. Keebler, E. L. Blickensderfer, And R. Besuijen, "Impact Of Alarm Management And Automation On Abnormal Operations: A Human-In-The-Loop Simulation Study," *Appl. Ergon.*, Vol. 100, P. 103670, Apr. 2022, doi: 10.1016/j.apergo.2021.103670.

[10] D. L. Zhang, L. Y. Xiao, Y. Wang, And G. Z. Huang, "Study On Vehicle Fire Safety: Statistic, Investigation Methods And Experimental Analysis," *Saf. Sci.*, Vol. 117, Pp. 194–204, Aug. 2019, doi: 10.1016/j.ssci.2019.03.030.

[11] J. Chojnowski And M. Karczewski, "Influence Of The Working Parameters Of The Chassis Dynamometer On The Assessment Of Tuning Of Dual-Fuel Systems," *Energies (Basel).*, Vol. 15, No. 13, P. 4869, Jul. 2022, doi: 10.3390/en15134869.

[12] C. Engström, P. Öberg, G. Fontaras, And B. Giechaskiel, "Considerations For Achieving Equivalence Between Hub- And Roller-Type Dynamometers For Vehicle Exhaust Emissions," *Energies (Basel).*, Vol. 15, No. 20, P. 7541, Oct. 2022, doi: 10.3390/en15207541.

[13] P. Doan, Đ. Thọ, T. T. Nguyen, And Tuan, "Study And Manufacturing Of Chassis Dynamometer For Motorcycle," *The Transport And Communications Science Journal*, Vol. 73, Pp. 316–326, Apr. 2022.

[14] J. C. Castillo, J. I. Huertas, M. Giraldo, A. F. Agudelo, And L. F. Quirama, "Equivalent Motorcycle Fuel Consumption And Emission Maps," *Energy Conversion And Management: X*, Vol. 31, P. 101951, Sep. 2026, doi: 10.1016/j.ecmx.2026.101951.

[15] J. F. Arifwardana, D. D. D. P. Tjahjana, M. Nizam, I. P. Rushadiawan, And M. R. A. Putra, "Performance Analysis And Characterization Hybrid Two Wheeller Vehicle With Using A Chassis Dynamometer," *Journal Of Electrical, Electronic, Information, And Communication Technology*, Vol. 6, No. 2, Pp. 64–68, 2024.

[16] S. Maniar, A. Umbarkar, And O. Morbale, "Performance Investigation Of Plc Hardware For Portable Two-Wheeler Dynamometer Test Rig," *Iop Conf. Ser. Mater. Sci. Eng.*, Vol. 1012, No. 1, P. 012047, Jan. 2021, doi: 10.1088/1757-899X/1012/1/012047.

[17] Z.-C. Dai, "Performance Verification Test Of Coaxial Centrifugal Clutch For Motorcycle Transmission System," *J. Phys. Conf. Ser.*, Vol. 2141, No. 1, P. 012008, Dec. 2021, doi: 10.1088/1742-6596/2141/1/012008.

[18] M. R. A. Putra, M. Nizam, D. D. D. P. Tjahjana, Z. Arifin, B. W. Lenggana, And I. Inayati, "Analysis Of Heat Generation On Unipolar Axial Eddy Current Brake Disc And Its Effect On Braking Performance," *World Electric Vehicle Journal*, Vol. 13, No. 10, P. 180, Sep. 2022, doi: 10.3390/wevj13100180.

[19] K. Zhang, Y. Lu, L. Chen, J. Bai, W. Dong, And J. Niu, "Design And Thermal Management Of A Novel Eddy Current Retarder For Electric Buses," *Proceedings Of The Institution Of Mechanical Engineers, Part D: Journal Of Automobile Engineering*, Vol. 240, No. 2–3, Pp. 837–847, Feb. 2026, doi: 10.1177/09544070251398577.

[20] Y. Xu *Et Al.*, "Reliability Of Mems Inertial Devices In Mechanical And Thermal Environments: A Review," *Heliyon*, Vol. 10, No. 5, P. E27481, Mar. 2024, doi: 10.1016/j.heliyon.2024.e27481.

[21] P. Fu, P. Yang, Z. Li, And J. Wang, "Temperature Characteristics Of Permanent Magnet Eddy Current Brake Under Overwinding Protection," *Journal Of Mechanical Science And Technology*, Vol. 40, No. 3, Pp. 2219–2226, Mar. 2026, doi: 10.1007/s12206-026-0257-2.

[22] L. Tan And Y. Yuan, "Assessment And Enhancement Of Scooter Thermal Management Via Integrated 1d-3d Simulation And Experimental Validation," *Proceedings Of The Institution Of Mechanical Engineers, Part D: Journal Of Automobile Engineering*, Feb. 2026, doi: 10.1177/09544070251411394.

[23] B. Giechaskiel, "Gaseous And Particulate Emissions Of A Euro 4 Motorcycle And Effect Of Driving Style And Open Or Closed Sampling Configuration," *Sustainability*, Vol. 12, No. 21, P. 9122, Nov. 2020, doi: 10.3390/su12219122.

[24] S. Bagaskoro And W. Aryadi, "Strength Analysis Of Rollers And Supports Of A Hydraulic Dynamometer Chassis Using Finite Element Method," *Jurnal Inovasi Mesin*, Vol. 6, No. 1, Pp. 1–8, Apr. 2024, doi: 10.15294/jim.v6i1.8961.

[25] H. Pranoto, B. Darmono, And G. Widyaputra, "Strength Analysis Of The Frame Structure With The Impact Load Between The Astm A36 And Jis G3101 Materials In The Electric Car E-Falco," *International Journal Of Advanced Technology In Mechanical, Mechatronics And Materials*, Vol. 3, No. 1, Pp. 26–38, Apr. 2022, doi: 10.37869/ijatec.v3i1.54.

[26] M. A. Sabtu, A. E. Admi, M. Mohamed Salleh, S. A. Osman, And S. A. Osman, "Finite Element Analysis Of Stress Distribution In Al6061 Frame Structures Under Varying Applied Loads," *International Journal Of Integrated Engineering*, Vol. 16, No. 2, Apr. 2024, doi: 10.30880/ijie.2024.16.02.027.

[27] M. Yazdi And S. Adumene, "Innovative Risk Management For Machine Safety: Insights From As/Nzs 4024 Standards," *The International Journal Of Advanced Manufacturing Technology*, Vol. 137, No. 1–2, Pp. 659–682, Mar. 2025, doi: 10.1007/s00170-025-15149-y.

[28] A.-R. Ioniță, D.-C. Anghel, And T. Boudouh, "Mind, Machine, And Meaning: Cognitive Ergonomics And Adaptive Interfaces In The Age Of Industry 5.0," *Applied Sciences*, Vol. 15, No. 14, P. 7703, Jul. 2025, doi: 10.3390/app15147703.

[29] J. Akyeampong, S. Udoka, G. Caruso, And M. Bordegoni, "Evaluation Of Hydraulic Excavator Human–Machine Interface Concepts Using Nasa Tlx," *Int. J. Ind. Ergon.*, Vol. 44, No. 3, Pp. 374–382, May 2014, doi: 10.1016/j.ergon.2013.12.002.

[30] S. Glimne, R. Brautaset, And C. Österman, "Visual Fatigue During Control Room Work In Process Industries," *Work: A Journal Of Prevention, Assessment & Rehabilitation*, Vol. 65, No. 4, Pp. 903–914, Apr. 2020, doi: 10.3233/WOR-203141.

[31] Dassault Systèmes, "Blended Curvature-Based Mesher," SOLIDWORKS Help.

[32] Dassault Systèmes, “Enhanced Blended Curvature-Based Mesher,” SOLIDWORKS Help.